Enthalpy-Driven RNA Folding: Single-Molecule Thermodynamics of Tetraloop−Receptor Tertiary Interaction[†]

Julie L. Fiore,[‡] Benedikt Kraemer,[§] Felix Koberling,[§] Rainer Edmann,[§] and David J. Nesbitt*[,‡]

JILA, National Institute of Standards and Technology and University of Colorado, Boulder, Colorado 80309, Department of Chemistry and Biochemistry, University of Colorado, Boulder, Colorado 80309, and PicoQuant, GmbH, Berlin, Germany 12489

Received October 21, 2008; Revised Manuscript Received January 28, 2009

ABSTRACT: RNA folding thermodynamics are crucial for structure prediction, which requires characterization of both enthalpic and entropic contributions of tertiary motifs to conformational stability. We explore the temperature dependence of RNA folding due to the ubiquitous GAAA tetraloop−receptor docking interaction, exploiting immobilized and freely diffusing single-molecule fluorescence resonance energy transfer (smFRET) methods. The equilibrium constant for intramolecular docking is obtained as a function of temperature ($T = 21-47$ °C), from which a van't Hoff analysis yields the enthalpy ($\Delta H°$) and entropy ($\Delta S°$) of docking. Tetraloop−receptor docking is significantly exothermic and entropically unfavorable in 1 mM $MgCl_2$ and 100 mM NaCl, with excellent agreement between immobilized ($\Delta H° = -17.4 \pm 1.6$ kcal/mol, and $\Delta S° = -56.2 \pm 5.4$ cal mol^{-1} K^{-1}) and freely diffusing ($\Delta H° = -17.2 \pm 1.6$ kcal/mol, and $\Delta S° = -55.9 \pm 5.2$ cal mol^{-1} K^{-1}) species. Kinetic heterogeneity in the tetraloop−receptor construct is unaffected over the temperature range investigated, indicating a large energy barrier for interconversion between the actively docking and nondocking subpopulations. Formation of the tetraloop−receptor interaction can account for ~60% of the $\Delta H°$ and $\Delta S°$ of P4−P6 domain folding in the *Tetrahymena* ribozyme, suggesting that it may act as a thermodynamic clamp for the domain. Comparison of the isolated tetraloop−receptor and other tertiary folding thermodynamics supports a theme that enthalpy- versus entropy-driven folding is determined by the number of hydrogen bonding and base stacking interactions.

RNA folding is generally hierarchical, with tertiary structure occurring through interactions of preformed secondary elements (*1*−*3*). As a result, the kinetics and thermodynamics of tertiary interactions are crucial to understanding RNA folding and functionality as well for accurate structural predictions (*1, 4*). Toward this end, individual folding motifs must be characterized both in isolation and in combination for a unifying thermodynamic description of RNA folding to emerge. Among the most widespread long-range RNA interactions are A-minor motifs (*5*−*7*), which are commonly manifested in GNRA tetraloop−receptor binding, where N is any nucleotide and R is a purine (*5, 8*). The ubiquitous GAAA tetraloop−receptor interaction has been of particular interest because it properly forms outside of the ribozyme's framework (*9, 10*). The GAAA tetraloop docks into an 11-nucleotide internal receptor (*11*), the bound and unbound structures of which have been extensively studied (*10*−*13*). There have been previous thermodynamic investigations of the tetraloop−receptor interaction in a variety of RNA folding contexts (*8, 14*−*18*). However, none of these studies has been able to isolate the enthalpy and entropy changes associated with tetraloop−receptor tertiary docking.

Enthalpies and entropies of tertiary structure formation can be obtained from the temperature dependence of equilibrium constants and/or precision calorimetry measurements. Differential scanning calorimetry has revealed enthalpy and free energy changes for pseudoknot tertiary folding (*19*). However, thermodynamics for tertiary structure formation can be challenging to isolate by methods such as isothermal titration calorimetry (ITC),[1] since studies are performed as a titration of two species, for which resolution of secondary and tertiary contributions is achieved through clever experimental design (*20*−*24*). Other ensemble methods for dissecting thermodynamic contributions to folding, such as temperature gradient gel electrophoresis, have had restricted application because experimental conditions are constrained by the limited resolution of gel shifts (*25*). Time-resolved ensemble FRET methods have been elegantly employed to probe tertiary folding thermodynamics, though data interpretation often requires preconceived models of fluorophore distance distributions, which potentially mask rare subpopulations (*26*).

[†] This work was supported in part by the NSF, NIST, the W. M. Keck Foundation initiative in RNA sciences at the University of Colorado, Boulder, and PicoQuant, GmbH. J.L.F. was supported in part by Optical Science and Engineering Program NSF-IGERT and CU Biophysics Training (T32 GM-065103) grants.

* To whom correspondence should be addressed: JILA, University of Colorado, 440 UCB, Boulder, CO 80309-0440. E-mail: djn@jila.colorado.edu. Phone: (303) 492-8857. Fax: (303) 492-5235.

[‡] JILA, National Institute of Standards and Technology and University of Colorado and Department of Chemistry and Biochemistry, University of Colorado.

[§] PicoQuant, GmbH.

[1] Abbreviations: HPLC, high-performance liquid chromatography; HEPES, *N*-(2-hydroxyethyl)piperazine-*N*′-2-ethanesulfonic acid; EDTA, ethylenediaminetetraacetate; ITC, isothermal titration calorimetry; NMR, nuclear magnetic resonance.

10.1021/bi8019788 CCC: $40.75
Published on Web 02/02/2009

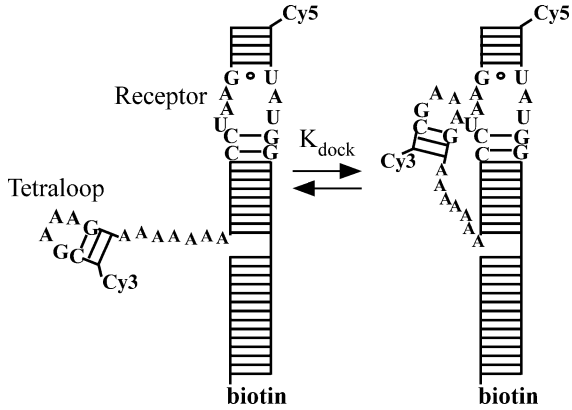

FIGURE 1: Secondary structure depiction of the tetraloop−receptor RNA docking−undocking equilibrium that can be observed by Cy3−Cy5 FRET. The undocked (left) GAAA tetraloop docks (right) into the receptor via a flexible A_7 linker, resulting in an increased FRET efficiency. Biotinylation of the RNA allows for immobilization on streptavidin-coated coverglass.

Single-molecule fluorescence resonance energy transfer (smFRET) methods have been widely applied to RNA folding (for recent reviews, see refs *27* and *28*). Such methods allow isolation and direct characterization of RNA tertiary conformational dynamics with subpopulations that exhibit different rate constants and conformations readily distinguished under a wide range of experimental conditions, e.g., varying Mg^{2+} concentrations (*16, 29, 30*). Despite the potential for temperature-dependent smFRET measurements of tertiary RNA folding thermodynamics, there have been surprisingly few such studies, specifically only P1 helix docking into the prefolded core of the *Tetrahymena* ribozyme and four-way helical junction folding (*31, 32*). Additionally, both of these smFRET studies have utilized surface-immobilized constructs.

In this work, we combine a microfluidic temperature-controlled stage with time-correlated single-photon counting methods in a confocal smFRET microscope to extract thermodynamic parameters for RNA folding under both freely diffusing and surface-immobilized conditions. We determine the standard state free energy ($\Delta G°$), enthalpy ($\Delta H°$), and entropy ($\Delta S°$) changes for intramolecular GAAA tetraloop−receptor docking under physiologically relevant cation conditions and identify the folding process as enthalpically driven but at a large entropic cost. We extract tertiary folding enthalpies and entropies by freely diffusing smFRET methods, which are advantageous because they require only trace amounts of sample while avoiding possible perturbative effects of surface tethering. Such freely diffusing methods have already yielded great insight into the secondary folding of RNA hairpins (*33*). We interpret the GAAA−tetraloop tertiary interaction in the context of previous thermodynamics studies to illuminate a possible enthalpic and entropic paradigm for RNA folding.

EXPERIMENTAL PROCEDURES

RNA Preparation. Cy3-Cy5-labeled tetraloop−receptor constructs depicted in Figure 1 were prepared as previously described (*15, 16*). Briefly, synthetic 5′-amino-modified RNA oligomers (Dharmacon, Lafayette, CO) are labeled with Cy3 and Cy5 N-succinimidyl esters (Amersham Biosciences, Piscataway, NJ) and HPLC-purified. The sequences of the RNA oligonucleotides are 5′ Cy5-GCC GAU AUG GAC GAC ACG CCC UCA GAC GAG UGC G 3′ and 5′ Cy3-GGC GAA AGC CAA AAA AAC GUG UCG UCC UAA GUC GGC 3′. We formed the complete construct (Figure 1) by annealing the Cy3 (1 μM) and Cy5 (1.5 μM) RNA oligomers with 2 μM biotinylated DNA oligomer (5′ biotin-CGC ACT CGT CTG AG 3′, Integrated DNA Technologies, Coralville, IA), heating the sample to 70 °C, and slowly cooling the sample to room temperature in an annealing buffer of 50 mM HEPES, 100 mM NaCl, and 100 μM EDTA (pH 7.5). The secondary structure of the Cy3 strand forms the tetraloop with an A_7 linker connecting it to the receptor domain created by the hybridized Cy3 and Cy5 strands. Molecules can be tethered to streptavidin-coated glass surfaces with the biotinylated extension formed by base pairing of the DNA and Cy5 strands. The micromolar stock of annealed RNA is diluted in working buffer that differs from the annealing buffer by the addition of 1 mM $MgCl_2$.

Single-Molecule Fluorescence Measurements. Immobilized or freely diffusing molecules are observed using a time-resolved confocal microscope system (Microtime 200, PicoQuant, GmbH) based on an inverted microscope (Olympus IX-71) equipped with a time-correlating single-photon counting module and objective scanning mode (P-721 PIFOC objective nanopositioner with x-y scanner P-733.2CL, Physik Instrumente, Karlsruhe, Germany). A 1.2 NA water-immersion objective (Olympus UPLSAPO 60XW) is used to focus a frequency-doubled pulsed picosecond (40 MHz) semiconductor laser at 532 nm (PicoTA, PicoQuant, GmbH) onto a glass surface for immobilized studies (1 μW at the microscope back plane, 1.7 kW/cm^2 at the focus) and 15 μm above the glass surface for freely diffusing studies (100 μW at the back plane, 170 kW/cm^2 at the focus). Fluorescence collected through the same objective is separated from the excitation source by a dichroic beamsplitter (Z532/635, Chroma Technology, Rockingham, VT) and focused through a 50 μm pinhole. Donor and acceptor emission are separated by a dichroic beamsplitter (645DCXR, Chroma Technology) and transmitted through bandpass filters (HQ585/70 M and HQ700/75M, Chroma Technology) for detection by single-photon counting avalanche photodiodes (SPCM-AQR-14, Perkin-Elmer). Data acquisition is achieved with a photon counting module (PicoHarp 300, PicoQuant, GmbH) in the time-tagged time-resolved mode, enabling the recording of every detected photon with its individual timing and detection channel information and processing with SymPhoTime (PicoQuant, GmbH).

Precise temperature control of the sample is achieved by implementation of a heated flow cell (FCS2, Bioptechs, Butler, PA) with an internal volume of 31 μL defined by a gasket spacer (0.1 mm × 14 mm × 27 mm) between the coverglass and a resistively heated, indium−tin oxide-coated slide (Bioptechs). The objective is heated to the same temperature as the flow cell to prevent a temperature gradient with respect to the immersion optic, with the objective thermally isolated from the microscope turret by a thermal spacer (Bioptechs). The reported temperatures and standard deviations are from an average over four point measurements: the top of the heated slide, on the coverglass in an immersion droplet, on the objective in an immersion droplet, and on the side of the objective. Temperatures are stable within ±0.2

°C during a given measurement, which are performed from ambient temperature to 47.4 °C.

Round No. 1.5 coverslips for the flow cell assembly are cleaned by rinsing with acetone, ethanol, HPLC-grade water, and then methanol followed by baking at 500 °C for 5 h. All experiments are performed in a buffer of 50 mM hemisodium HEPES (pH 7.5 at 25 °C), 100 mM NaCl, 100 μM ETDA, and 1 mM $MgCl_2$. HEPES is a temperature stable buffer with only minor changes in pH with temperature ($\Delta pK_a = -0.014\ °C^{-1}$), indicating a pH reduction to 7.22 at 45 °C (*34*). Immobilized samples are prepared in the FCS2 holder using a biotinylated BSA−streptavidin−biotinylated RNA tethering scheme (*35*). An enzymatic oxygen scavenging solution of glucose (9 mg/mL), glucose oxidase (0.43 mg/mL), catalase (0.072 mg/mL), and 2 mM Trolox is added to the buffer to reduce fluorophore photobleaching and photophysics (*36*). For freely diffusing measurements, the glass surfaces are passivated with BSA and experiments are performed with a 200 pM RNA solution in the holder (*37*). The oxygen scavenging system is not used in the freely diffusing experiments as it was found to offer no advantage at the powers used (*37*).

Single-Molecule FRET Efficiency Analysis. Immobilized single-molecule trajectories are analyzed with 10 ms data binning, which clearly resolves the undocked and docked events (*16, 37*). Freely diffusing time traces are analyzed with 1 ms integration times, which is on the order of a molecule's dwell time in the laser focus (*16, 37*). As previously derived, the corrected intensity-based FRET efficiency (E_{FRET}) is calculated from the background-subtracted signals on the two channels, ΔI_1 and ΔI_2, designed primarily for donor and acceptor detection, respectively. Corrections are implemented for (i) collection efficiencies and cross talk of the donor and acceptor emission on channels 1 and 2 (β_1^A, β_2^A, β_1^D, and β_2^D), (ii) differential quantum yields of the donor and acceptor (Q_D and Q_A), and (iii) fractional direct excitation of the acceptor versus donor (α_A, where $1 - \alpha_D = \alpha_A$)

$$E_{FRET} = \frac{\beta_1^D \Delta I_2 - \beta_2^D \Delta I_1 - \frac{\alpha_A}{\alpha_D}\frac{Q_A}{Q_D}(\beta_2^A \Delta I_1 - \beta_1^A \Delta I_2)}{\beta_1^D \Delta I_2 - \beta_2^D \Delta I_1 + \frac{Q_A}{Q_D}(\beta_2^A \Delta I_1 - \beta_1^A \Delta I_2)} \quad (1)$$

Quantum yield ratios and collection efficiencies are determined in independent measurements of singly labeled constructs: $Q_A/Q_D = 1.2 \pm 0.3$, $\beta_1^A = 0.00000 \pm 0.00003$, $\beta_2^A = 0.0242 \pm 0.0018$, $\beta_1^D = 0.0269 \pm 0.0024$, and $\beta_2^D = 0.00211 \pm 0.00018$ (*37*). Fractional direct laser excitation of the acceptor and donor is calculated from the extinction coefficients at 532 nm ($\alpha_A = 0.07 \pm 0.01$, and $\alpha_D = 0.93 \pm 0.01$) (*37*). In contrast to the immobilized studies, donor-only species in the freely diffusing studies are necessarily included and appear at negative E_{FRET} values due to correction for acceptor direct excitation (*37*).

RESULTS

Temperature Dependence of Tetraloop−Receptor Docking Equilibrium Revealed in Single-Molecule Trajectories. The docking−undocking equilibrium of the GAAA tetraloop and receptor is readily monitored by FRET between the donor (Cy3) and acceptor (Cy5) in the RNA construct (Figure 1), as described elsewhere (*16*). The tetraloop is flexibly attached to the receptor domain with a single-stranded A_7 linker, which was previously shown to allow for an isolated thermodynamic study of a tertiary interaction (*15, 16*). Temperature-dependent conformational dynamics in single-immobilized molecules under physiological conditions [100 mM NaCl, 1 mM $MgCl_2$, and 50 mM HEPES (pH 7.5)] are observed in E_{FRET} trajectories calculated ratiometrically from real-time donor and acceptor fluorescence signals (see Experimental Procedures) (*16, 37*). Sample trajectories portraying the temperature dependence of the tetraloop−receptor docking equilibrium are shown in Figure 2. Fluctuations between undocked (low E_{FRET}) and docked (high E_{FRET}) conformations are visible in each of the time traces (*16*). Probability distributions from the E_{FRET} trajectories allow two states to be distinguished (right panel, Figure 2).

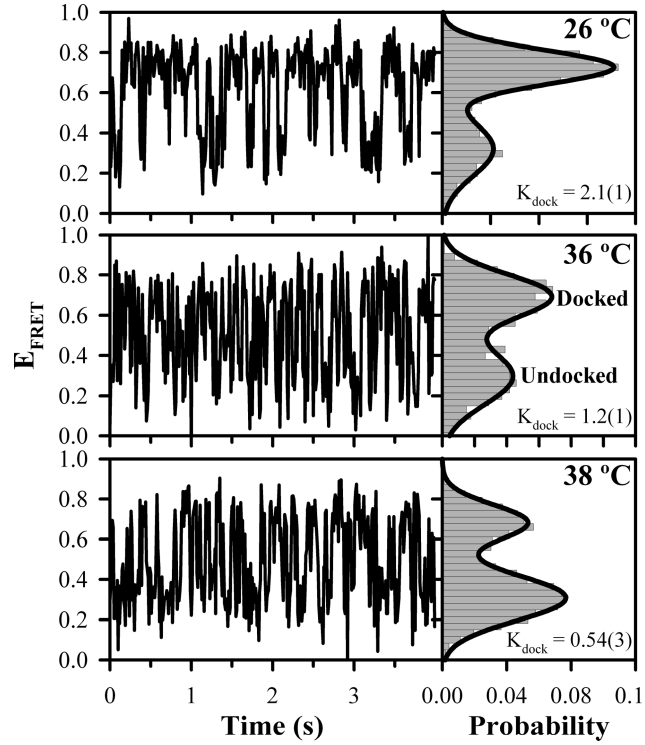

FIGURE 2: Immobilized single-molecule E_{FRET} trajectories and the corresponding probability distributions at 26 (top), 36 (middle), and 38 °C (bottom). The low and high E_{FRET} peaks correspond to the undocked and docked states, respectively. Integrated areas of the undocked and docked peaks are determined from the superimposed two-Gaussian fits with the equilibrium constant for docking, K_{dock}, calculated as the ratio of the docked to undocked area. Increasing temperature shifts the equilibrium to the undocked state.

The E_{FRET} probability histograms are described well by Gaussian distributions (*37*); fitting the histograms to a sum of Gaussians permits quantitation of relative docked versus undocked populations. From cumulative probability distributions of many molecules, we determine $\langle E_{FRET} \rangle = 0.29 \pm 0.02$ and 0.70 ± 0.02 and width $\sigma = 0.14 \pm 0.01$ and 0.094 ± 0.003 for the undocked and docked states, respectively, in excellent agreement with previous studies of this construct (*37*). The E_{FRET} centers ($\langle E_{FRET} \rangle$) and Gaussian widths (σ) for the molecules shown in Figure 2 at 26, 36, and 38 °C show no systematic shifts as the temperature is increased, indicating that (i) obscuring of docked and undocked peaks

due to finite binning is negligible and (ii) the tetraloop and receptor secondary structure are maintained upon heating, since disruption of these regions would lead to shifts in the E_{FRET} peaks. Secondary structure is expected be unaffected in this study as both the tetraloop and receptor domains are extremely stable; the melting temperature (T_m) of the tetraloop domain was experimentally determined at ~64 °C (*38*), and the T_m of the receptor domain is predicted to be ~62 °C from the DINAMelt server (*39*). Furthermore, the robustness of the E_{FRET} peak position suggests fluorophore quantum yields are sufficiently independent of temperature over the range measured.

The effect of temperature on fluorophore quantum yields is independently assessed on singly labeled constructs at the experimental extremes. Comparison of relative quantum yields at 21 and 45 °C shows a decrease of ~20% for both Cy3 and Cy5 as the RNA is heated over this range; the quantum yield effect is reversible as observed by temperature cycling. A similar diminution of Cy3 quantum yield has also been observed by Levitus and co-workers for Cy3−DNA conjugates (*40*). Quantum yield changes induce a 2-fold effect on the observed E_{FRET}, where $E_{FRET} = R_0^6/(R_0^6 + R^6)$, both through the Förster radius (R_0) and in the E_{FRET} calculation from emission intensities (see eq 1) for a defined distance (R). The latter contribution is negligible in the ratiometric determination of E_{FRET} as the relative ratio Q_A/Q_D does not change (see eq 1). The R_0 effect is also subtle because R_0 is proportional to $Q_D^{1/6}$ (*41*). For the observed decrease of ~20% in donor quantum yield, we predict an E_{FRET} center decrease of only ~0.03 for undocked and docked peaks over the entire temperature range investigated (see Figure S1 of the Supporting Information). Such a peak shift may be present but is on the order of E_{FRET} center reproducibility (±0.02) and not relevant within experimental uncertainty. Furthermore, absolute positions of these peaks have no effect on the analysis presented here as we seek only the relative areas of the docked and undocked peaks, which are populated on the basis of the fractional dwell time of the molecule in each configuration.

The calculated fluorophore distance from the corrected E_{FRET} in the docked conformation is consistent with proper formation of the tetraloop−receptor interaction as observed in the X-ray crystal structure of the P4−P6 domain of the *Tetrahymena* ribozyme (*11*). The interphosphate distance between the corresponding nucleotides to which the fluorophores would be attached in the P4−P6 domain is 31.6 Å. Our observed E_{FRET} of 0.29 corresponds to an R of 46 Å in the docked state for an R_0 of 53.4 Å [$R^6 = R_0^6(1/E_{FRET} - 1)$]. The functionalized fluorophores are attached to amino-modified RNA with a three-carbon linker, which places 12 atoms between each fluorophore and its nucleotide phosphate. This added distance can easily account for the additional 14.4 Å between Cy3 and Cy5 as compared to the interphosphate distance in P4−P6, though the exact position of the fluorophores in this construct is not structurally known. The observed E_{FRET} for the undocked conformation also indicates a distance (R = 62 Å) that is consistent with a right angle extension of the tetraloop A_7 arm with respect to the receptor helix (R ~ 70 Å). However, inferring absolute distances from FRET efficiencies is challenging because fluorophore rotation is potentially hindered upon covalent attachment to biomolecules. Hindered rotation affects R_0, which is calculated assuming free rotation (i.e., κ^2 is assumed to be $^2/_3$), though this assumption is spurious as shown in recent studies by Lilley and co-workers (*42*). Nevertheless, observed E_{FRET} values are in agreement with the anticipated unfolded and folded conformations of the tetraloop−receptor construct.

Table 1: Temperature Dependence of K_{dock} and Thermodynamic Parameters for Tetraloop−Receptor Docking from Immobilized and Freely Diffusing (free) Single-Molecule Methods

T (°C)	K_{dock}(immobilized)	K_{dock}(free)	$\Delta G°$ (kcal/mol) = $-RT \ln K_{dock}$
21 ± 0.2	4.18 ± 0.18	3.7 ± 1.8	−0.80 ± 0.05
26 ± 0.2	2.3 ± 0.1	−	−0.50 ± 0.03
29 ± 0.2	2.2 ± 0.2	1.7 ± 0.3	−0.4 ± 0.1
34 ± 2	1.32 ± 0.08	0.87 ± 0.16	−0.05 ± 0.16
36 ± 2	1.17 ± 0.09	−	−0.10 ± 0.05
38 ± 2	0.64 ± 0.03	0.60 ± 0.11	0.30 ± 0.03
43 ± 3	−	0.55 ± 0.10	0.43 ± 0.12
47.4 ± 3.6	−	0.42 ± 0.09	0.58 ± 0.12

	immobilized	free
$\Delta H°$ (kcal/mol)	−17.4 ± 1.6	−17.2 ± 1.6
$\Delta S°$ (cal mol^{-1} K^{-1})	−56.2 ± 5.4	−55.9 ± 5.2

The undocked and docked conformations of the tetraloop receptor are clearly assigned, allowing determination of equilibrium constants from the ratios of integrated peak areas (K_{dock} = area docked/area undocked), which is the fractional dwell time in the docked versus undocked state (*18*). An enhanced tendency for tetraloop−receptor constructs to be in the undocked conformation with an increase in temperature is apparent from the single-molecule traces, with K_{dock} decreasing from 2.1 ± 0.1 at 26 °C to 0.54 ± 0.03 at 38 °C (Figure 2). Cumulative K_{dock} values for many molecules are in good agreement with the individual molecules (see Figure 2) and summarized over the full temperature range (21.0−47.4 °C) in Table 1 [K_{dock}(immobilized)], indicating a strongly exothermic folding process.

Significant kinetic heterogeneity exists in the tetraloop−receptor system, as discussed previously (*16*). This heterogeneity can be adequately described as two non-interconverting populations: (i) 68% of species that actively dock and undock, and (ii) a 32% minority population of molecules that exhibit no folding events. The presence of "nondocking" molecules was also confirmed under freely diffusing conditions, yielding a 32% subpopulation in quantitative agreement with the tethered studies (*37*). Since these molecules show no docking events over the range of time scales and temperatures sampled, they are excluded from the equilibrium analysis described above. The molecular origin of the species is not yet known, e.g., whether the kinetic trap is of secondary or tertiary origin. These molecules never achieve the bound form of the tetraloop receptor so cannot be included in assessing tetraloop−receptor thermodynamics. Studies have suggested that the nondockers can be removed from the sample by native gel electrophoresis (*15*); however, we retain them in the study, to assess whether they can interconvert at increased temperatures. Temperatures greater than investigated may allow the nondockers to fold, which would be consistent with the remarkable robustness of subpopulations in the hairpin ribozyme (*43*). Further confirmation of the temperature insensitivity of the nondocking RNA subpopulation is provided by studies under freely diffusing conditions as described below.

Temperature Dependence of the Docking Equilibrium in Freely Diffusing RNA. For temperature-dependent measurements of the tetraloop−-receptor interaction without surface immobilization, the equilibrium conformational distribution of the tetraloop−receptor construct is acquired from individual molecules freely diffusing through the confocal detection volume. This method allows for rapid sampling of many molecules, but with the ability to still discern conformational states (*37*). Low concentrations (200 pM) of RNA ensure that we are in the single-molecule detection regime, which is confirmed by cross correlation analysis of the donor and acceptor channels for freely diffusing time traces (see Figure S2 of the Supporting Information), yielding an average occupancy of the focal volume of 0.71 ± 0.09 molecule. Cross correlations also indicate the concentration of donor- and acceptor-labeled species is maintained upon heating, indicating that RNA construct remains intact. Time traces are binned at 1 ms integration for analysis, which is on the order of the dwell time of a molecule in the detection volume (*37*). This bin time is much shorter than the typical duration of a docking or undocking event; thus, a molecule can be cleanly identified in either the undocked or docked conformation (*16*). Fluorescence emission from labeled RNA molecules is distinguished from background via an intensity threshold ($I_{thresh} = 10\sigma_{background} = 30$ kHz) of a minimum sum of photons above background levels with typically $>10^4$ events acquired to ensure high-quality statistics (*44*). In freely diffusing studies, all fluorescent species in the solution are sampled. Therefore, signals from donor-only molecules give rise to a peak at negative E_{FRET} due to direct excitation correction for the missing or photobleached acceptor (see Experimental Procedures) (*37*). As illustrated in Figure 3, the donor-only population shows no change with temperature, consistent with the RNA constructs remaining hybridized throughout temperature cycling.

The freely diffusing E_{FRET} histogram data can be globally fit over all temperatures by a sum of Gaussian distributions with common widths and centers, confirming that the docked and undocked peak shapes and positions are not significantly affected by heating. Such an analysis yields an $\langle E_{FRET}\rangle_{undocked}$ of 0.291 ± 0.003 and a $\sigma_{undocked}$ of 0.153 ± 0.004, and an $\langle E_{FRET}\rangle_{docked}$ of 0.679 ± 0.004 and a σ_{docked} of 0.112 ± 0.003, in agreement with the above immobilized results and previous freely diffusing studies at room temperature ($\langle E_{FRET}\rangle$ = 0.28 ± 0.01 and 0.687 ± 0.005 and σ = 0.165 ± 0.004 and 0.106 ± 0.002 for undocked and docked states, respectively) (*37*). Temperature and immobilization, therefore, do not introduce any observable changes in FRET centers and widths for both the undocked and docked RNA conformations, indicating that the system is described well by a two-state reaction scheme under all conditions in these studies. As demonstrated in Figure 3, the docked and undocked E_{FRET} amplitudes do display temperature sensitivity. Specifically, increased temperature shifts the tetraloop−receptor construct to the undocked conformation, which is quantified by extracting K_{dock} from the equilibrium distributions. Extracting equilibrium constants from the threshold event distribution is potentially only an estimate of K_{dock} because of preferential detection of molecules dominantly emitting photons from the fluorophore with higher net collection efficiency. However, systematic variation of the threshold (15−75 kHz) reveals a negligible effect on the results presented. Such a result is expected as the collection efficiencies and quantum yields of the donor and acceptor are nearly equivalent in our experimental apparatus (see Experimental Procedures).

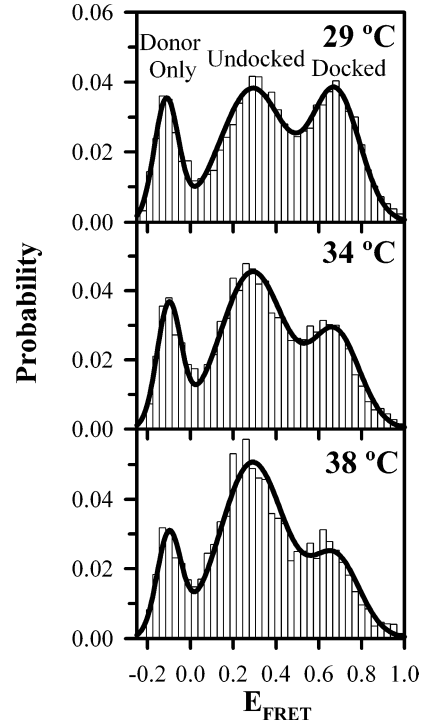

FIGURE 3: Temperature dependence of tetraloop−receptor docking shown in E_{FRET} histograms generated from photon bursts occurring when freely diffusing RNAs traverse the laser focal volume (see Experimental Procedures). Three distinct populations with peaks corresponding to the donor-only ($E_{FRET} < 0$), undocked (center E_{FRET} = 0.291 ± 0.003), and docked RNA (center E_{FRET} = 0.679 ± 0.004) exist at 29, 34, and 38 °C. There is a marked increase in the relative fraction of the undocked population with temperature, indicating disruption of the tertiary interaction, which is quantified by fitting the histograms to a sum of Gaussian distributions (solid black lines).

The freely diffusing detection method samples an equilibrium conformational distribution of all tetraloop−receptor constructs, including both actively docking (68%) and nondocking (32%) subpopulations. The nondocking subpopulation can be incorporated in the analysis by noting that the fractional population in the docked state (F_{free}) must scale linearly (i.e., $F_{free} = \alpha F_{immobilized}$) with the fractional docked state populations under immobilized conditions, where nondocking molecules are excluded (*37*). This fraction can be written explicitly as

$$F_{free} = \frac{N_{docked}}{N_{docked} + N_{undocked} + N_{nondock}} = \alpha\frac{N_{docked}}{N_{docked} + N_{undocked}} = \alpha\frac{K_{dock}}{K_{dock} + 1} \quad (2)$$

where N_{docked} and $N_{undocked} + N_{nondock}$ are integrated areas of docked and undocked peaks in freely diffusing studies, respectively. The actively docking fraction, α, has been previously measured for both immobilized (α = 0.68 ± 0.01)

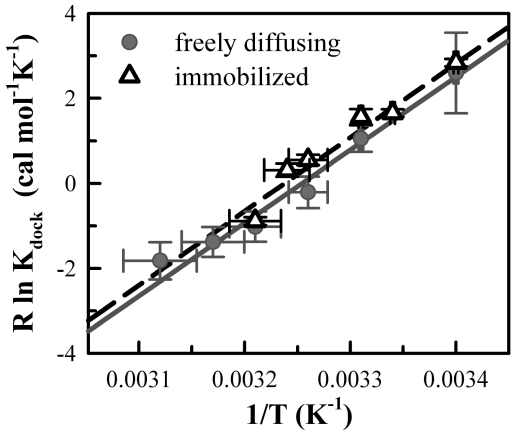

FIGURE 4: Thermodynamics of the tetraloop−receptor docking−undocking equilibrium from van't Hoff plots (see eq 4). The temperature (T) dependence of the docking equilibrium constant (K_{dock}) is shown for freely diffusing (gray circles) and immobilized (black open triangles) molecules. Linear fits of R ln K_{dock} vs $1/T$ yield a slope of $-\Delta H°$ and an intercept of $\Delta S°$ (see Table 1) for the freely diffusing (solid gray line) and immobilized (dashed black line) data.

(*37*) and freely diffusing ($\alpha = 0.66 \pm 0.02$) species (*37*). As a result, K_{dock} is readily extracted from F_{free} by

$$K_{dock} = \frac{F_{free}}{\alpha - F_{free}} \quad (3)$$

where the nondocking fraction is identified by immobilized studies to be independent of temperature. As summarized in Table 1, K_{dock} under diffusing conditions decreases from 3.7 ± 1.8 at 21 °C to 0.42 ± 0.09 at 47 °C. The equilibrium constants are in agreement for freely diffusing and immobilized constructs, confirming that the nondocking fraction is constant over this temperature range.

Thermodynamics for Tetraloop−Receptor Docking. To extract thermodynamic information from these two independent methods, we analyze both the immobilized and diffusing data sets according to the van't Hoff equation

$$R \ln K_{dock} = -\frac{\Delta H°}{T} + \Delta S° \quad (4)$$

from which a plot of R ln K_{dock} versus $1/T$ yields a slope of $-\Delta H°$ and an intercept of $\Delta S°$ (see Figure 4), where R is the gas constant (1.987 cal mol^{-1} K^{-1}). Both data sets yield straight line van't Hoff plots, of which least-squares fits weighted for uncertainty of the dependent and independent variables yield the following: $\Delta H°_{immobilized} = -17.4 \pm 1.6$ kcal/mol, $\Delta H°_{free} = -17.2 \pm 1.6$ kcal/mol, $\Delta S°_{immobilized} = -56.2 \pm 5.4$ cal mol^{-1} K^{-1}, and $\Delta S°_{free} = -55.9 \pm 5.2$ cal mol^{-1} K^{-1}, which can be converted to standard international units with the conversion factor 4.184 J/cal. Freely diffusing and immobilized approaches for characterizing the thermodynamics of the tetraloop−receptor tertiary interaction are in excellent agreement (Figure 4). Docking of the tetraloop with the receptor results in a substantial decrease in enthalpy with an unfavorable entropy change (i.e., "enthalpy-driven folding"), where exothermicity is balanced at room temperature by a high entropic cost. More quantitatively, the standard state free energy ($\Delta G°$) for forming the tetraloop−receptor interaction can be directly calculated as a function of temperature from the equilibrium constants ($\Delta G° = -RT$ ln K_{dock}), as summarized in Table 1. At 21 °C, the docked state is only marginally favored ($\Delta G° = -0.08 \pm 0.05$ kcal/mol), with docking becoming thermodynamically unfavorable at physiological temperatures (≈37 °C).

DISCUSSION

Accurate thermodynamic characterization of tertiary RNA folding is clearly important but has been extremely limited (*15*−*17, 31*). We demonstrate the applicability of temperature-dependent smFRET methods under both immobilized and freely diffusing conditions in deconstructing the docking thermodynamics for an isolated tetraloop−receptor tertiary motif. Freely diffusing techniques are particularly useful for monitoring RNA folding thermodynamics in the absence of surface tethering, which was demonstrated for the exothermic and entropically disfavored secondary folding of isolated RNA hairpins (*33*). We determine the standard state enthalpic and entropic components of tetraloop−receptor binding, revealing that the tertiary interaction like the secondary hairpin formation is enthalpy-driven, but at a large entropic cost. Extension of these methods to other isolated tertiary interactions and comparison to RNAs with multiple interactions should permit valuable insights into, for example, the thermodynamic origin of tertiary cooperativity (*18, 45*). Such dissections of RNA folding interactions are applicable to well-defined, modular components as in this scheme. Such a "bottom up" approach complements studies in large RNAs by avoiding potentially deleterious mutations that may disrupt the tertiary interaction through changes in global structure.

NMR and X-ray crystal structures of the docked and undocked tetraloop and receptor reveal structural contributions to the entropic cost and enthalpic favorability of tetraloop−receptor association. Specifically, tetraloop−receptor docking induces structural elements that have been generally recognized as enthalpically stabilizing and entropically unfavorable, namely, hydrogen bonding and base stacking interactions (*10, 11, 46, 47*). The large entropic penalty for folding may also originate from the loss of free orientational flexibility of the tetraloop in the undocked state to the specific orientation required for docking (*11, 13*). The proposition that the flexibility in an unfolded structure is correlated with the entropic cost of folding is supported by thermodynamic studies of the hairpin ribozyme, in which a four-way junction (4WJ) greatly decreased the entropic penalty of folding as compared to the two-way junction (2WJ). The 4WJ contributes significant rigidity and orientation to the unfolded state, leading to a decrease in the level of disorder prior to the docking event (*26*). Solvent effects, such as disruption of ordered water molecules, yield positive enthalpic and entropic folding contributions; this is opposite to what is observed for tetraloop−receptor folding and therefore not the dominant effect (*48*).

Although the measured enthalpy and entropy changes are dominated by the tetraloop−receptor interaction, we also consider thermodynamic contributions arising from the RNA construct design. Specifically, contributions could arise from the flexible A_7 linker because of small differences in its base stacking in the docked and undocked forms. Additional negative entropic contributions to folding due to the reduced conformational space accessible to the linker in the docked versus undocked states are expected to be modest because

Table 2: Thermodynamic Parameters for Tetraloop−Receptor Docking and Other Tertiary Folding (4.184 J/cal)

RNA tertiary interaction	conditions	$\Delta H°$ (kcal/mol)	$\Delta S°$ (cal mol^{-1} K^{-1})	$\Delta G°$ at 37 °C = $\Delta H° - T\Delta S°$ (kcal/mol)
tetraloop−receptor docking	immobilized, 1 mM $MgCl_2$, 0.1 M NaCl	−17.4 ± 1.6	−56.2 ± 5.4	0.02 ± 2.3
	freely diffusing, 1 mM $MgCl_2$, 0.1 M NaCl	−17.2 ± 1.6	−55.9 ± 5.2	0.13 ± 2.3
P4−P6 domain folding(*25*)	0.9 mM $MgCl_2$, 10 mM NaCl	−28 ± 3	−91 ± 8	0.21 ± 3.9
hairpin ribozyme folding (*26*)	2WJ, 1 mM $MgCl_2$	−9.7 ± 4.5	−34 ± 17	0.84 ± 7
	4WJ, 1 mM $MgCl_2$	−4.1 ± 2.3	−9.6 ± 5.7	−1.1 ± 2.9
P1 helix docking into *Tetrahymena* group I intron core	10 mM $MgCl_2$ (*31*)	8 ± 2	25 ± 8	0.25 ± 3.2
	5 mM $MgCl_2$, 135 mM NaCl (*53*)	8	40	−4
	10 mM $MgCl_2$ (*54*)	19 ± 9	62 ± 30	−0.22 ± 13
3WJ folding of hammerhead ribozyme core (*21*)	10 mM $MgCl_2$, 0.1 M NaCl	41 ± 1	120 ± 10	3.8 ± 3.3

this region is sufficiently long to maintain disorder. By way of confirmation, previous studies of linker length (A_7 vs A_{14}) and composition (A vs U) dependence of tetraloop−receptor docking and undocking revealed minimal changes in the equilibrium constant (*15, 16*).

Our results allow us to place the tetraloop−receptor interaction in thermodynamic context with global folding of the P4−P6 domain in the *Tetrahymena* ribozyme, which has been studied at the ensemble level by temperature gradient gel electrophoresis under similar cation conditions (see Table 2) (*25*). Results for the global fold indicate large net enthalpy and entropy decreases of −28 ± 3 kcal/mol ($\Delta H°$) and −91 ± 8 cal mol^{-1} K^{-1} ($\Delta S°$), respectively, i.e., also enthalpically driven with a magnitude only slightly larger than the tetraloop−receptor values. Although there are additional tertiary interactions and structural complexity to consider in the full P4−P6 folding problem, it would appear that the GAAA tetralop−receptor construct alone may contribute ≈60% of the $\Delta H°$ and $\Delta S°$. The tetraloop−receptor interaction has been proposed as a thermodynamic clamp for stabilizing the global fold of large RNAs (*17*). This work supports such a picture by determining that thermodynamic stability may originate from the strongly favorable tetraloop−receptor docking enthalpy. Further inspection will be necessary to evaluate how the complexity of large RNAs affects the folding thermodynamics, with assessment of the role of global architecture, secondary elements, and solvent accessibility.

However, the docked form of the tetraloop−receptor construct is thermodynamically disfavored (i.e., $\Delta G°_{\text{immobilized,free}} = 0.022 \pm 2.3$ or 0.13 ± 2.3 kcal/mol) under physiologically relevant conditions (37 °C, 1 mM $MgCl_2$, 100 mM NaCl), with similar results for the P4−P6 domain ($\Delta G° = 0.21 \pm 3.9$ kcal/mol). This borderline stability of even strongly enthalpy-driven folding underscores that RNA folding dynamics must be addressed for a complete understanding of functionality. Folding of both P4−P6 domain and the tetraloop−receptor construct becomes favorable with increased Mg^{2+} concentrations (*16, 18*).

The thermodynamic parameters for P4−P6 and tetraloop−receptor folding are consistent with that of other RNA folding, specifically global folding of tRNA (*49*), the 1051−1108 rRNA fragment (*50*), the hairpin ribozyme (*26*), pseudoknot tertiary structure formation (*19*), ligand-induced riboswitch folding (*51*), and secondary loop formation (*33, 52*). Although differing in magnitude, each of these systems exhibits significant enthalpic gain ($\Delta H° < 0$) and entropic penalty ($\Delta S° < 0$) for folding. Furthermore, in a recent ITC study, Reymond et al. demonstrated through systematic mutations that various steps in the folding pathway of the hepatitis delta virus ribozyme are exothermic and entropically disfavored (*24*). However, these observations of enthalpy-driven RNA folding are not a universal trend, as evidenced in Table 2. The final stage of *Tetrahymena* ribozyme folding, i.e., the docking of the P1 duplex into the prefolded core, was investigated by smFRET of immobilized molecules and found to be enthalpically disfavored ($\Delta H° = 8 \pm 2$ kcal/mol) and entropically favored ($\Delta S° = 25 \pm 8$ cal mol^{-1} K^{-1}), in reasonable agreement with ensemble methods (*53, 54*). ITC studies of the three-way junction (3WJ) in the minimal hammerhead ribozyme core reveal a similar degree of endothermicity and entropic advantage (Table 2) (*21*). As yet a third case, smFRET investigation of the hairpin ribozyme's 4WJ revealed no temperature dependence in the folding equilibrium constants, from which one can infer the processes to be nearly thermoneutral ($\Delta H° \approx 0$ kcal/mol) with only a modest decrease in disorder ($\Delta S° \approx -2 \pm 1$ cal mol^{-1} K^{-1}) between the various folded conformations (*32*).

As illustrated in Table 2, each tertiary association has a $\Delta G°$ near zero; thus, RNA folding can be regarded as either enthalpy- or entropy-driven. Folding events in the tetraloop−receptor, P4−P6 domain, and hairpin ribozyme constructs result in many hydrogen bonds and base stacking interactions, of which tetraloop−receptor docking forms the fewest, i.e., 10 hydrogen bonds and improved base stacking (*10, 11, 55*). By way of contrast, such enthalpy-driven interactions are much less prevalent in the entropy-driven P1 docking, which nets only four or five hydrogen bonds and no base stacking (*56*). The reduced prevalence of these secondary-like interactions (i.e., from ∼11 to 4) may account for the shift from enthalpy-driven to entropy-driven (solvent-driven) folding. The net entropic drive for this folding has been proposed to arise from displacement of ordered water molecules and/or Mg^{2+} ions (*53, 54*). Furthermore, the *Tetrahymena* ribozyme is already highly structured prior to P1 docking, which reduces the entropic cost associated with the final folding transition.

Folding of the minimal hammerhead ribozyme is more difficult to categorize in terms of base stacking and hydrogen bonding because the structure of the core prior to coaxial stacking of the helices is not clear. However, counting hydrogen bonds and base stacking interactions that are contingent on helix alignment, i.e., not including the two noncanonical base pairs (A_9-G_{12} and G_8-A_{13}) that likely form in the core prior to helical stacking, we identify a net of approximately seven interactions (*57, 58*). This is intermediate, albeit closer to the case of P1 than tetraloop−receptor docking; therefore, solvent effects, e.g., displacement of ordered water molecules, are not overcome, and entropy increases in minimal hammerhead ribozyme folding (*21, 53, 54*). Endothermic changes are associated with rearrangement of core residues of the hammerhead ribozyme (*21*), which may explain the additional enthalpic penalty for

hammerhead core folding versus P1 docking. In summary, the data suggest that categorization of enthalpy- versus entropy-driven RNA folding arises from competing roles of solvent and hydrogen bonding and stacking interactions, with a net ~11 interactions providing sufficient negative $\Delta H°$ and $\Delta S°$ to overcome solvent effects. Furthermore, each of the entropy-driven RNA folds (see Table 2), as well as the thermoneutral 4WJ, was measured at significantly higher concentrations of Mg^{2+} than the enthalpy-driven cases [>10 mM vs ~1 mM Mg^{2+} (see Table 2)]. A Mg^{2+} environment that is more amenable to RNA folding, though less physiological, may also contribute to the observation of entropy-driven folding by increasing the magnitude of solvent effects. Further systematic study of isolated tertiary motifs with temperature-dependent smFRET methods will be invaluable in further elucidating the competing roles of solvent and hydrogen bonding and stacking interaction to categorize enthalpy- versus entropy-driven RNA folding.

As a final comment, in the course of preparing this work, we became aware of a simultaneous and independent ITC investigation of tetraloop−receptor binding by the Butcher group. Specifically, the Butcher group had cleverly designed pairs of RNA constructs, based on back-to-back copies of tetraloops (TT) and receptors (RR). These constructs can form a duplex (TRTR) through dual tetraloop−receptor docking, which permits association to be initiated by mixing of the two constructs. This work by Vander Meulen et al. published elsewhere (*23*) yields a $\Delta H°$ of -33.2 ± 2.0 kcal/mol at 45 °C for double tetraloop−receptor formation under similar solvent conditions (2 mM $MgCl_2$, 20 mM KCl). Assuming zero enthalpy cooperativity between the two tertiary interactions, this translates into a $\Delta H°_{ITC}$ of -16.9 ± 1.0 kcal/mol for single tetraloop−receptor binding, which agrees with our single-molecule values of -17.2 ± 1.6 kcal/mol ($\Delta H°_{free}$) and -17.4 ± 1.6 kcal/mol ($\Delta H°_{immobilized}$). This agreement between isolated and dual tetraloop−receptor docking enthalpies supports a picture in which tertiary structure formation in RNA may be largely enthalpically noncooperative. In turn, this would imply an entropic origin of tertiary cooperativity between the tetraloop−receptor and metal−core interactions observed in folding of the complete P4−P6 domain (*18*).

CONCLUSION

Thermodynamics of the isolated GAAA tetraloop−receptor tertiary interaction are investigated at the single-molecule level, exploiting the combination of temperature-dependent FRET and confocal microscopy methods. Results for the GAAA tetraloop−receptor motif are shown to be enthalpically driven ($\Delta H_{free} = -17.2 \pm 1.6$ kcal/mol, and $\Delta H_{immobilized} = -17.4 \pm 1.6$ kcal/mol) yet balanced by entropically unfavorable ($\Delta S_{free} = -55.9 \pm 5.2$ cal mol^{-1} K^{-1}, and $\Delta S_{immobilized} = -56.2 \pm 5.4$ cal mol^{-1} K^{-1}) conformational changes upon docking. These results for tetraloop−receptor folding already achieve 60% of the values obtained from ensemble studies for folding of the complete P4−P6 domain, supporting previous views that the tetraloop−receptor construct provides a dominant source of thermodynamic stabilization. However, under physiological temperature conditions, this isolated tertiary motif is found to be marginally unstable ($\Delta G = 0.02$ and 0.13 kcal/mol from immobilized and freely diffusing, respectively), indicating that conformational change may still play a key role in RNA functionality. Further work on temperature and cation dependences of the rates, k_{dock} and k_{undock}, will be necessary to illuminate the transition state enthalpy and entropy changes associated with tertiary contact formation and to help develop a consensus picture for the thermodynamic origin of cation-mediated RNA folding.

ACKNOWLEDGMENT

We thank Bioptechs for their generous technical support of this study and valuable discussions. We also thank Drs. Arthur Pardi and Christopher D. Downey for their contributions to the RNA construct design and many helpful comments in the preparation of the manuscript.

SUPPORTING INFORMATION AVAILABLE

Prediction of the effect of donor quantum yield (Q_D) on the observed FRET efficiency (E_{FRET}) as a function of Cy3−Cy5 distance (R) (Figure S1) and mean cross correlations of donor and acceptor channels for the same sample containing tetraloop−receptor constructs under freely diffusing single-molecule conditions at 21 and 45 °C (Figure S2). This material is available free of charge via the Internet at http://pubs.acs.org.

REFERENCES

1. Tinoco, I., and Bustamante, C. (1999) How RNA folds. *J. Mol. Biol. 293*, 271–281.
2. Greenleaf, W. J., Frieda, K. L., Foster, D. A. N., Woodside, M. T., and Block, S. M. (2008) Direct observation of hierarchical folding in single riboswitch aptamers. *Science 319*, 630–633.
3. Brion, P., and Westhof, E. (1997) Hierarchy and dynamics of RNA folding. *Annu. Rev. Biophys. Biomol. Struct. 26*, 113–137.
4. Leontis, N. B., Lescoute, A., and Westhof, E. (2006) The building blocks and motifs of RNA architecture. *Curr. Opin. Struct. Biol. 16*, 279–287.
5. Lee, J. C., Gutell, R. R., and Russell, R. (2006) The UAA/GAN internal loop motif: A new RNA structural element that forms a cross-strand AAA stack and long-range tertiary interactions. *J. Mol. Biol. 360*, 978–988.
6. Nissen, P., Ippolito, J. A., Ban, N., Moore, P. B., and Steitz, T. A. (2001) RNA tertiary interactions in the large ribosomal subunit: The A-minor motif. *Proc. Natl. Acad. Sci. U.S.A. 98*, 4899–4903.
7. Doherty, E. A., Batey, R. T., Masquida, B., and Doudna, J. A. (2001) A universal mode of helix packing in RNA. *Nat. Struct. Biol. 8*, 339–343.
8. Abramovitz, D. L., and Pyle, A. M. (1997) Remarkable morphological variability of a common RNA folding motif: The GNRA tetraloop-receptor interaction. *J. Mol. Biol. 266*, 493–506.
9. Qin, P. Z., Butcher, S. E., Feigon, J., and Hubbell, W. L. (2001) Quantitative analysis of the isolated GAAA tetraloop/receptor interaction in solution: A site-directed spin labeling study. *Biochemistry 40*, 6929–6936.
10. Butcher, S. E., Dieckmann, T., and Feigon, J. (1997) Solution structure of a GAAA tetraloop receptor RNA. *EMBO J. 16*, 7490–7499.
11. Cate, J. H., Gooding, A. R., Podell, E., Zhou, K. H., Golden, B. L., Kundrot, C. E., Cech, T. R., and Doudna, J. A. (1996) Crystal structure of a group I ribozyme domain: Principles of RNA packing. *Science 273*, 1678–1685.
12. Jucker, F. M., and Pardi, A. (1995) GNRA tetraloops make a U-Turn. *RNA 1*, 219–222.
13. Davis, J. H., Tonelli, M., Scott, L. G., Jaeger, L., Williamson, J. R., and Butcher, S. E. (2005) RNA helical packing in solution: NMR structure of a 30 kDa GAAA tetraloop-receptor complex. *J. Mol. Biol. 351*, 371–382.
14. Jaeger, L., and Leontis, N. B. (2000) Tecto-RNA: One-dimensional self-assembly through tertiary interactions. *Angew. Chem., Int. Ed. 39*, 2521–2524.

15. Downey, C. D., Fiore, J. L., Stoddard, C. D., Hodak, J. H., Nesbitt, D. J., and Pardi, A. (2006) Metal ion dependence, thermodynamics, and kinetics for intramolecular docking of a GAAA tetraloop and receptor connected by a flexible linker. *Biochemistry 45*, 3664–3673.
16. Hodak, J. H., Downey, C. D., Fiore, J. L., Pardi, A., and Nesbitt, D. J. (2005) Docking kinetics and equilibrium of a GAAA tetraloop-receptor motif probed by single-molecule FRET. *Proc. Natl. Acad. Sci. U.S.A. 102*, 10505–10510.
17. Young, B. T., and Silverman, S. K. (2002) The GAAA tetraloop-receptor interaction contributes differentially to folding thermodynamics and kinetics for the P4-P6 RNA domain. *Biochemistry 41*, 12271–12276.
18. Sattin, B. D., Zhao, W., Travers, K., Chut, S., and Herschlag, D. (2008) Direct measurement of tertiary contact cooperativity in RNA folding. *J. Am. Chem. Soc. 130*, 6085–6087.
19. Nixon, P. L., and Giedroc, D. P. (2000) Energetics of a strongly pH dependent RNA tertiary structure in a frameshifting pseudoknot. *J. Mol. Biol. 296*, 659–671.
20. Hammann, C., Cooper, A., and Lilley, D. M. J. (2001) Thermodynamics of ion-induced RNA folding in the hammerhead ribozyme: An isothermal titration calorimetric study. *Biochemistry 40*, 1423–1429.
21. Mikulecky, P. J., Takach, J. C., and Feig, A. L. (2004) Entropy-driven folding of an RNA helical junction: An isothermal titration calorimetric analysis of the hammerhead ribozyme. *Biochemistry 43*, 5870–5881.
22. Feig, A. L. (2007) Applications of isothermal titration calorimetry in RNA biochemistry and biophysics. *Biopolymers 87*, 293–301.
23. Vander Meulen, K. A., Davis, J. H., Foster, T. R., Record, T., and Butcher, S. E. (2008) Thermodynamics and folding pathway of tetraloop receptor-mediated RNA helical packing. *J. Mol. Biol. 384*, 702–717.
24. Reymond, C., Bisaillon, M., and Perreault, J.-P. (2009) Monitoring of an RNA multistep folding pathway by isothermal titration calorimetry. *Biophys. J. 96*, 132.
25. Szewczak, A. A., Podell, E. R., Bevilacqua, P. C., and Cech, T. R. (1998) Thermodynamic stability of the P4-P6 domain RNA tertiary structure measured by temperature gradient gel electrophoresis. *Biochemistry 37*, 11162–11170.
26. Klostermeier, D., and Millar, D. P. (2000) Helical junctions as determinants for RNA folding: Origin of tertiary structure stability of the hairpin ribozyme. *Biochemistry 39*, 12970–12978.
27. Li, P. T. X., Vieregg, J., and Tinoco, I. (2008) How RNA unfolds and refolds. *Annu. Rev. Biochem. 77*, 77–100.
28. Bokinsky, G., and Zhuang, X. W. (2005) Single-molecule RNA folding. *Acc. Chem. Res. 38*, 566–573.
29. Zhuang, X. W., Kim, H., Pereira, M. J. B., Babcock, H. P., Walter, N. G., and Chu, S. (2002) Correlating structural dynamics and function in single ribozyme molecules. *Science 296*, 1473–1476.
30. Xie, Z., Srividya, N., Sosnick, T. R., Pan, T., and Scherer, N. F. (2004) Single-molecule studies highlight conformational heterogeneity in the early folding steps of a large ribozyme. *Proc. Natl. Acad. Sci. U.S.A. 101*, 534–539.
31. Bartley, L. E., Zhuang, X. W., Das, R., Chu, S., and Herschlag, D. (2003) Exploration of the transition state for tertiary structure formation between an RNA helix and a large structured RNA. *J. Mol. Biol. 328*, 1011–1026.
32. Hohng, S., Wilson, T. J., Tan, E., Clegg, R. M., Lilley, D. M. J., and Ha, T. J. (2004) Conformational flexibility of four-way junctions in RNA. *J. Mol. Biol. 336*, 69–79.
33. Gell, C., Sabir, T., Westwood, J., Rashid, A., Smith, D. A. M., Harris, S.-A., and Stockley, P. G. (2008) Single-Molecule Fluorescence Resonance Energy Transfer Assays Reveal Heterogeneous Folding Ensembles in a Simple RNA Stem-Loop. *J. Mol. Biol. 384*, 264–278.
34. Good, N. E., Winget, G. D., Winter, W., Connolly, T. N., Izawa, S., and Singh, R. M. M. (1966) Hydrogen ion buffers for biological research. *Biochemistry 5*, 467–477.
35. Ha, T., Zhuang, X. W., Kim, H. D., Orr, J. W., Williamson, J. R., and Chu, S. (1999) Ligand-induced conformational changes observed in single RNA molecules. *Proc. Natl. Acad. Sci. U.S.A. 96*, 9077–9082.
36. Rasnik, I., McKinney, S. A., and Ha, T. (2006) Nonblinking and longlasting single-molecule fluorescence imaging. *Nat. Methods 3*, 891–893.
37. Fiore, J. L., Hodak, J. H., Piestert, O., Downey, C. D., and Nesbitt, D. J. (2008) Monovalent and divalent promoted GAAA-tetraloop-receptor tertiary interactions from freely diffusing single-molecule studies. *Biophys. J. 95*, 3892–3905.
38. Hernández, B., Baumruk, V., Leulliot, N., Gouyette, C., Huynh-Dinh, T., and Ghomi, M. (2003) Thermodynamic and structural features of ultrastable DNA and RNA hairpins. *J. Mol. Struct. 651−653*, 67–74.
39. Markham, N. R., and Zuker, M. (2005) DINAMelt web server for nucleic acid melting prediction. *Nucleic Acids Res. 33*, W577–W581.
40. Sanborn, M. E., Connolly, B. K., Gurunathan, K., and Levitus, M. (2007) Fluorescence Properties and Photophysics of the Sulfoindocyanine Cy3 Linked Covalently to DNA. *J. Phys. Chem. B 111*, 11064–11074.
41. Förster, T. (1948) Zwischenmolekulare Energiewanderung und Fluoreszenz. *Ann. Phys. (Weinheim, Ger.) 2*, 55–75.
42. Iqbal, A., Arslan, S., Okumus, B., Wilson, T. J., Giraud, G., Norman, D. G., Ha, T., and Lilley, D. M. J. (2008) Orientation dependence in fluorescent energy transfer between Cy3 and Cy5 terminally attached to double-stranded nucleic acids. *Proc. Natl. Acad. Sci. U.S.A. 105*, 11176–11181.
43. Ditzler, M. A., Rueda, D., Mo, J., Hakansson, K., and Walter, N. G. (2008) A rugged free energy landscape separates multiple functional RNA folds throughout denaturation. *Nucleic Acids Res.* doi: 10.1093/nar/gkn871.
44. Deniz, A. A., Dahan, M., Grunwell, J. R., Ha, T. J., Faulhaber, A. E., Chemla, D. S., Weiss, S., and Schultz, P. G. (1999) Single-pair fluorescence resonance energy transfer on freely diffusing molecules: Observation of Forster distance dependence and subpopulations. *Proc. Natl. Acad. Sci. U.S.A. 96*, 3670–3675.
45. Chauhan, S., and Woodson, S. A. (2008) Tertiary interactions determine the accuracy of RNA folding. *J. Am. Chem. Soc. 130*, 1296–1303.
46. Serra, M. J., Turner, D. H., Michael, L. J., and Ackers, G. K. (1995) Predicting thermodynamic properties of RNA. *Methods Enzymol. 259*, 242–261.
47. Silverman, S. K., and Cech, T. R. (1999) Energetics and cooperativity of tertiary hydrogen bonds in RNA structure. *Biochemistry 38*, 8691–8702.
48. Mikulecky, P. J., and Feig, A. L. (2006) Heat capacity changes associated with nucleic acid folding. *Biopolymers 82*, 38–58.
49. Stein, A., and Crothers, D. M. (1976) Conformational-changes of transfer-RNA: Role of magnesium(II). *Biochemistry 15*, 160–168.
50. Lu, M., and Draper, D. E. (1994) Bases defining an ammonium and magnesium ion-dependent tertiary structure within the large subunit ribosomal-RNA. *J. Mol. Biol. 244*, 572–585.
51. Stoddard, C. D., Gilbert, S. D., and Batey, R. T. (2008) Ligand-dependent folding of the three-way junction in the purine riboswitch. *RNA 14*, 675–684.
52. Antao, V. P., and Tinoco, I. (1992) Thermodynamic parameters for loop formation in RNA and DNA hairpin tetraloops. *Nucleic Acids Res. 20*, 819–824.
53. Li, Y., Bevilacqua, P. C., Mathews, D., and Turner, D. H. (1995) Thermodynamic and activation parameters for binding of a pyrene-labeled substrate by the *Tetrahymena* ribozyme: Docking is not diffusion-controlled and is driven by a favorable entropy. *Biochemistry 34*, 14394–14399.
54. Narlikar, G. J., and Herschlag, D. (1996) Isolation of a local tertiary folding transition in the context of a globally folded RNA. *Nat. Struct. Biol. 3*, 701–710.
55. Rupert, P. B., and Ferre-D'Amare, A. R. (2001) Crystal structure of a hairpin ribozyme-inhibitor complex with implications for catalysis. *Nature 410*, 780–786.
56. Szewczak, A. A., Ortoleva-Donnelly, L., Ryder, S. P., Moncoeur, E., and Strobel, S. A. (1998) A minor groove RNA triple helix within the catalytic core of a group I intron. *Nat. Struct. Biol. 5*, 1037–1042.
57. Pley, H. W., Flaherty, K. M., and McKay, D. B. (1994) 3-Dimensional structure of a hammerhead ribozyme. *Nature 372*, 68–74.
58. Scott, W. G., Finch, J. T., and Klug, A. (1995) The crystal structure of an All-RNA hammerhead ribozyme: A proposed mechanism for RNA catalytic cleavage. *Cell 81*, 991–1002.

BI8019788